Acta Crystallographica Section F
Structural Biology and Crystallization Communications
ISSN 1744-3091

Crystallization of a challenging antigen–antibody complex: TLR3 ECD with three noncompeting Fabs

Thomas J. Malia,* Galina Obmolova, Jinquan Luo, Alexey Teplyakov, Raymond Sweet and Gary L. Gilliland*

Centocor R&D, 145 King of Prussia Road, Radnor, PA 19087, USA

Correspondence e-mail: tmalia@its.jnj.com, ggillila@its.jnj.com

Received 6 June 2011
Accepted 2 August 2011

The mechanism of action of therapeutic antibodies can be elucidated from the three-dimensional crystal structures of their complexes with antigens, but crystallization remains the primary bottleneck to structure determination. Methods that resulted in the successful crystallization of TLR3 ECD in complex with Fab fragments from three noncompeting, neutralizing anti-TLR3 antibodies are presented. The crystallization of this 238 kDa complex was achieved through fine purification of the quaternary complex of TLR3 with the three Fab fragments combined with microseed matrix screening and additive screening. Fine purification entailed the application of a very shallow gradient in anion-exchange chromatography, resulting in the resolution of two separate complex peaks which had different crystallizabilities. Subsequent structure determination defined the epitopes of the respective antibodies and revealed a mechanistic hypothesis that is currently under investigation. The results also showed that cocrystallization with multiple noncompeting Fab fragments can be a viable path when an antigen complex with a single Fab proves to be recalcitrant to crystallization.

1. Introduction

There are numerous strategies for overcoming the challenges of protein crystallization, such as exploiting different mechanisms of crystal growth, various seeding techniques and the use of crystallization chaperones (Chayen & Saridakis, 2008; McPherson, 2004). Crystallization is most commonly performed by vapor diffusion (Benvenuti & Mangani, 2007), but other mechanisms can be employed such as microbatch under oil, microdialysis, free-interface diffusion and microfluidic crystallization depending on the particular problem (Chayen & Saridakis, 2008). Once initial crystallization conditions have been discovered, microseeding has shown remarkable success in many cases for improving crystal quality (Bergfors, 2003). A variation of microseeding that has shown great applicability is microseed matrix screening (MMS), in which crystalline microseeds are introduced into different conditions from those of the original crystal seeds. Such an approach uncouples nucleation from crystal growth and is used to discover conditions for growth that are quite distinct from those found in the initial crystallization screen (D'Arcy *et al.*, 2007; Ireton & Stoddard, 2004; Obmolova *et al.*, 2010). Another tool to consider for very challenging targets such as membrane proteins are crystallization chaperones (Hunte & Michel, 2002; Kovari *et al.*, 1995; Rasmussen *et al.*, 2007; Zhou *et al.*, 2001). Crystallization chaperones are auxiliary proteins, typically antibody fragments, that bind with high affinity to target molecules and enhance crystallizability (Koide, 2009). An additional strategy that can improve crystallization success is the fine purification of complexes to minimize heterogeneity.

These approaches and strategies were applied in the structural investigation of TLR3 and antibodies that inhibit its signaling required for an innate immune response. TLR3 is an innate immune receptor that recognizes and is activated by double-stranded RNA

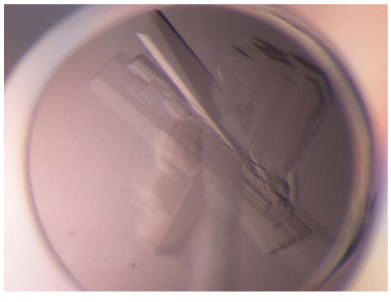

(Alexopoulou *et al.*, 2001). We have developed three noncompeting inhibitory monoclonal antibodies against this receptor with affinities in the 100–500 p*M* range. In order to understand their mechanisms of action, we set out to determine the crystal structures of the extracellular domain (ECD) of TLR3 in complex with one or more of the Fab fragments of the monoclonal antibodies (Fab15, Fab12 and Fab1068). Extensive crystallization trials coupled with a number of purification methods and seeding combinations yielded diffraction-quality crystals only for the quaternary complex of TLR3 ECD with the three Fabs (TLR3+3Fab). In this communication, we describe the approach that led to the successful crystallization of the TLR3+3Fab complex.

2. Materials and methods

2.1. Proteins

The gene encoding human TLR3 ECD (residues 22–702 of NCBI accession No. NP_003256) and a C-terminal 6×His tag was amplified by PCR with 5′ *Bam*HI and 3′ *Bgl*II restriction sites. This fragment was inserted into the pAcgp67A (BD Biosciences) baculovirus expression vector. The resulting transfer vector was co-transfected with BaculoGOLD linearized baculovirus DNA (BD Biosciences) into Sf9 cells to produce a recombinant baculovirus encoding human TLR3 ECD. TLR3 ECD was produced at Proteos (Kalamazoo, Michigan, USA) by expression in Sf9 insect cells and was purified by immobilized metal-affinity chromatography (IMAC; HisTrap). The protein was dialyzed into 20 m*M* Tris pH 7.4, 50 m*M* NaCl (Xtal buffer) for crystallization.

Fab vector construction and expression was performed according to Zhao *et al.* (2009). The heavy-chain and light-chain Fab fragments of Fab12, Fab15 and Fab1068 were cloned into mammalian expression vectors, coexpressed in HEK cells, purified by IMAC (HisTrap, GE Life Sciences) and size-exclusion chromatography (SEC), and dialyzed into Xtal buffer. Fab1068 is composed of the Fv of CNTO2424 chimerized onto human CH and Cκ constant domains (Duffy *et al.*, 2007).

Proteins were analyzed by SDS–PAGE using NuPAGE 4–12% Bis-Tris gels with NuPAGE MES SDS running buffer (Invitrogen) under nonreducing conditions.

2.2. Protein deglycosylation

TLR3 ECD in Xtal buffer was exchanged into 50 m*M* sodium phosphate pH 5.5 and deglycosylated with Endo H (Sigma) at 303 K for 17 h. The reaction was monitored for completion by SDS–PAGE and MALDI. Deglycosylated TLR3 ECD was purified by anion-exchange chromatography on a Mono Q 5/50 GL column (GE Life Sciences) pre-equilibrated in 20 m*M* Tris pH 7.5, 5% glycerol, 2 m*M* DTT, 1 m*M* EDTA and eluted with a 1.5–2.2% gradient of 20 m*M* Tris pH 7.5, 5% glycerol, 2 m*M* DTT, 1 m*M* EDTA, 1 *M* NaCl over 50 column volumes.

2.3. Protein-complex purification

The TLR3+3Fab complex was prepared by mixing TLR3 ECD with all three Fabs, each at a 1.0:1.1 molar ratio, and incubating at 277 K for 2–4 h. Protein complexes were purified by SEC and anion-exchange chromatography.

The TLR3+3Fab complex was purified by SEC on a Superdex 200 HiLoad 16/60 column (GE Life Sciences) at 1 ml min^{-1} in 20 m*M* HEPES pH 7.5, 0.1 *M* NaCl. The SEC-purified TLR3+3Fab complex was concentrated to approximately 9 mg ml^{-1} for crystallization. The SEC-purified complex was additionally purified by anion-exchange chromatography under reducing conditions using a Mono Q 5/50 GL column equilibrated in 20 m*M* Tris pH 8.5, 10% glycerol, 1 m*M* DTT. Approximately 1.6 mg complex was diluted fivefold with equilibration buffer and eluted at 0.5 ml min^{-1} with a linear gradient of 0–10% 20 m*M* Tris pH 8.5, 10% glycerol, 1 m*M* DTT, 1 *M* NaCl over 30 column volumes. The main peak was pooled, buffer-exchanged to 20 m*M* Tris pH 8.5, 50 m*M* NaCl and concentrated to 8 mg ml^{-1} for crystallization trials.

Anion exchange under nonreducing conditions was performed on a Mono Q 5/50 GL column (GE Life Sciences) equilibrated with 20 m*M* Tris pH 8.5, 10% glycerol (buffer *A*). Approximately 2.5 mg of the TLR3+3Fab complex was diluted tenfold with buffer *A* and loaded onto the column at 0.5 ml min^{-1}. The TLR3+3Fab complex was eluted at 0.5 ml min^{-1} with a linear gradient of 0–10% 20 m*M* Tris pH 8.5, 10% glycerol, 1 *M* NaCl (buffer *B*) over 40 column volumes. Peak 1 and peak 2 were pooled separately and concentrated to approximately 14 mg ml^{-1} in a final buffer consisting of 20 m*M* Tris pH 8.5, 10% glycerol and 30 m*M* NaCl for crystallization.

Proteins were concentrated using an Amicon Ultra 10 000 molecular-weight cutoff device (Millipore). The protein concentration of complexes was determined spectrophotometrically at 280 nm using an extinction coefficient calculated from the amino-acid content of all components, E = 289 970 M^{-1} cm $^{-1}$, for the quaternary complex.

2.4. Complex crystallization

Automated crystallization screening was performed using an Oryx4 crystallization robot (Douglas Instruments) dispensing equal volumes of protein and reservoir solution (0.2 µl each) in sitting-drop format using Corning 3550 plates (Corning Inc.). Microseed matrix screening (MMS) was performed using the Oryx4 robot by dispensing components in the following ratio: 0.2 µl protein:0.05 µl seeds:0.15 µl reservoir solution. Crystallization screening for the complex was performed with Crystal Screen HT, PEG/Ion HT (Hampton Research), in-house 96-condition screens IH1 and IH2 (G. Obmolova *et al.*, manuscript in preparation) and optimization screens. Crystallization trials were performed at 293 K.

Additive screening combined with MMS was performed sequentially using the Oryx4 robot by first mixing 0.2 µl protein, 0.05 µl seeds and 0.15 µl reservoir solution immediately followed by mixing 0.2 µl protein, 0.08 µl additive and 0.12 µl reservoir solution into the previous drops containing seeds. The final ratio of the components was 1:0.125:0.2:0.675 protein:seeds:additive:reservoir solution.

2.5. Seed preparation

Seeds were prepared by mechanical homogenization using the Seed Bead Kit (Hampton Research) according to the manufacturer's protocol. Seed stocks were prepared by mixing crystals from different but chemically related conditions. Sodium formate seeds were prepared by combining IH1 G3 (MES pH 6.5, 4.5 *M* sodium formate), IH1 G4 (MES pH 6.5, 5.8 *M* sodium formate) and IH1 H4 (Tris pH 8.5, 5.8 *M* sodium formate). Ammonium sulfate seeds were combined from in-house and refinement screens and prepared in a stabilizing solution consisting of 0.1 *M* sodium acetate pH 4.5, 3.0 *M* ammonium sulfate.

2.6. X-ray diffraction data collection

For X-ray data collection, a crystal (of dimensions ∼1.0 × 0.5 × 0.1 mm) was soaked for a few seconds in a synthetic mother liquor

(0.1 *M* sodium acetate pH 4.5, 28% PEG 3350, 1 *M* LiCl, 16% glycerol) and flash-cooled in a stream of nitrogen at 100 K. X-ray diffraction data were collected and processed using a Rigaku MicroMax-007 HF microfocus X-ray generator equipped with Osmic VariMax confocal optics, a Saturn 944 CCD detector and an X-stream 2000 cryocooling system (Rigaku, The Woodlands, Texas, USA). Diffraction intensities were detected over a 250° crystal rotation with an exposure time of 1 min per 0.5° image to the maximum resolution of 5 Å. X-ray data were processed with the program *d*TREK* (Pflugrath, 1999).

3. Results and discussion

Our general approach to the crystallization of antibody–antigen complexes is as follows. Protein-purification methods are explored to determine the most suitable approach for obtaining a homogenous complex for crystallization trials. This determination is most often performed in conjunction with crystallization screening to assess the quality of the purified complex for forming crystals. Multiple purification methods may be assessed in parallel. Initial crystallization screening is performed with commercial sparse-matrix screens and in-house footprint-type screens. After the initial screenings of the antigen–antibody complex crystals are often obtained, but they are usually not suitable for diffraction studies so further refinement is necessary. Refinement incorporates the highly successful method of microseed matrix screening (MMS; D'Arcy *et al.*, 2007; Ireton & Stoddard, 2004). Hits containing needles, plates or microcrystals are selected for pooling into crystallization seed stocks. For MMS, these seeds are then incorporated into the original sparse-matrix and footprint screens as well as the optimization screens. Seeding is used throughout screening in order to both accelerate crystal growth and to conserve the purified complex by using a relatively lower concentration of the complex. While purification strategies are being evaluated for improvement of crystallization, new sources of seeds can be accumulated. In the case of TLR3+Fab, multiple combinations of TLR3 with different Fabs were evaluated in order to determine the most suitable complex. When crystals are of sufficient size and quality, X-ray diffraction propensity is evaluated. If diffraction is poor, attempts to further improve crystal quality can be made by additive screening using compounds from different chemical classes (for example, detergents, linkers, amphiphiles and carbohydrates).

Our goal was to determine the structural epitope and paratope of three different neutralizing TLR3 antibodies *via* X-ray crystallography. To this end, the crystallization of different combinations of Fabs complexed with the TLR3 ECD were attempted. This included all seven possible combinations of TLR3 ECD–Fab complexes (binary, ternary and quaternary). Similar purification (SEC, ion-exchange chromatography) followed by standard crystallization screening was performed for all of these complexes. The TLR3+3Fab complex gave the only promising hit in the initial screen and no crystallization hits were obtained with the various other complexes. Therefore, further crystallization efforts were focused on the quaternary complex, which we describe below.

3.1. Size-exclusion chromatography and crystallization screening

SEC separated a major peak corresponding to the quaternary complex and minor peaks owing to excess Fabs (Fig. 1*a*). The major peak was pooled and concentrated and crystallization trials were set up. No useful crystallization hits were found from the crystallization trials of the SEC-purified TLR3+3Fab complex, so additional sample-preparation methods were pursued.

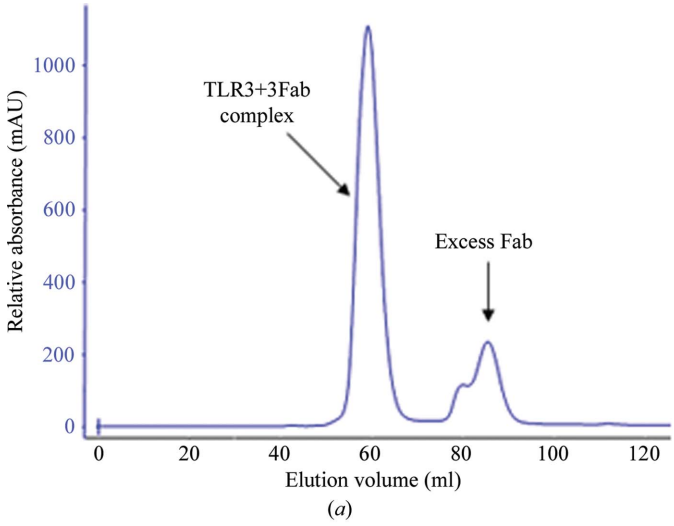

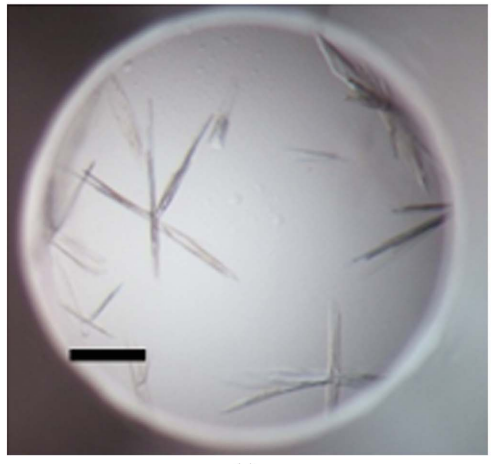
(c)

Figure 1
(*a*) SEC profile of TLR3+3Fab. TLR3+3Fab complex elution volume: 59.35 ml. Calibration standards (not shown): thyroglobulin (670 kDa), 50.33 ml; γ-globulin (158 kDa), 66.79 ml; ovalbumin (44 kDa), 82.45 ml; myoglobin (17 kDa), 94.68 ml; vitamin B_{12} (1.35 kDa), 111.90 ml. (*b*) Anion-exchange purification of the TLR3+3Fab complex in the presence of 1 m*M* DTT. Pooled fractions (blue box) and aggregate are indicated. (*c*) Needle-like crystals of the TLR3+3Fab complex from initial screening (0.1 *M* sodium acetate pH 4.5, 2.4 *M* ammonium sulfate, 5% PEG 400). The scale bar is 0.2 mm in length.

3.2. Ion-exchange purification and crystallization screening

A reducing agent was employed in the purification of TLR3 ECD for both published structures, presumably to prevent disulfide-mediated aggregation (Bell *et al.*, 2005; Choe *et al.*, 2005). Therefore, a similar approach was attempted in ion-exchange purification of the complex. The SEC-purified complex of TLR3+3Fab was further purified by anion exchange in the presence of 1 m*M* DTT, which removed aggregates (Fig. 1*b*). From initial screening of this ion-exchange-purified complex, the first protein crystals of the TLR3+3Fab complex were observed (Fig. 1*c*). Seeds were prepared from these crystals and a subsequent round of MMS was performed using the same screens as the initial screening. After MMS a number of the experiments produced small crystals under different conditions. Crystals from ammonium sulfate and sodium formate conditions were combined into a Seed Mix for further MMS. We combined these seeding solutions because we were not sure which seeds would facilitate crystal growth.

In order to further improve homogeneity, the TLR3+3Fab complex was purified by anion exchange under nonreducing conditions employing a 0–10% gradient of buffer *B* over 40 column volumes. With this shallow gradient and relatively low protein loading, two peaks could be resolved (Figs. 2 and 3). In order to obtain sufficient purified complex for crystallization trials, multiple runs were performed in succession. While peak 1 appears to run at a slightly higher molecular weight than peak 2 on SDS–PAGE (Fig. 3), we were unable to determine the differences between the two peaks by mass spectrometry; however, both peaks contained TLR3+3Fab. Crystallization trials were set up separately for protein collected from both peaks. MMS was performed with the two samples using IH1 and IH2 screens with the Seed Mix. Two hits were identified for both peaks: (i) 0.1 *M* sodium acetate 4.5, 2.8 *M* ammonium sulfate, 5% PEG 400 and (ii) 0.1 *M* sodium acetate pH 4.5, PEG 3350, 1 *M* LiCl.

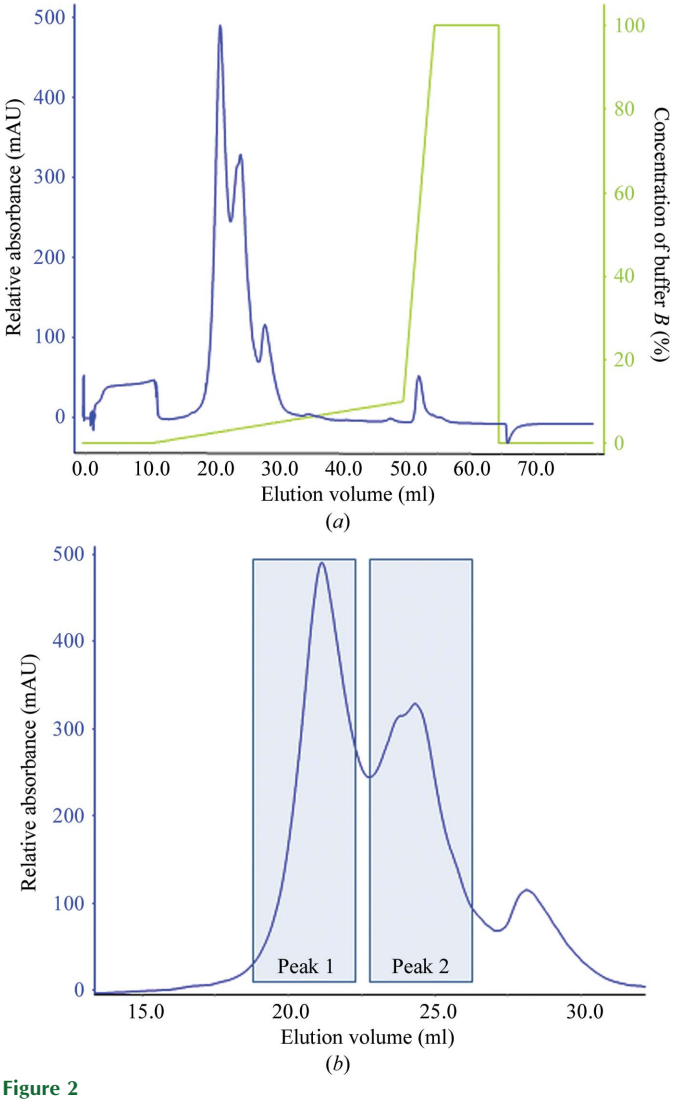

Figure 2
(*a*) Anion-exchange purification profile of TLR3+3Fab under nonreducing conditions. (*b*) Expansions of the main peak and pooled fractions.

3.3. Deglycosylated TLR3+3Fab complex

TLR3 ECD contains approximately 16.8 kDa glycan as determined by MALDI mass spectrometry. Endo H deglycosylation removed approximately 3.1 kDa of glycan. A complex of deglycosylated TLR3 ECD with three Fabs was formed and purified by anion-exchange chromatography under nonreducing conditions (Fig. 3, lane 8). A screen consisting of similar conditions that gave hits for the glycosylated complex was set up with MMS. A large crystal was found from 0.1 *M* acetate pH 4.5, 26.4% PEG 3350, 1 *M* LiCl; however, it only diffracted to >15 Å resolution. This condition could not be optimized further. The deglycosylated complex was more susceptible to precipitation, which suggests that the glycans promote solubility and their removal leads to instability of TLR3 and the complex.

3.4. Refinement screening and additive screening

A refinement screen including ammonium sulfate conditions and PEG 3350/1 *M* LiCl conditions was set up for peak 1 and peak 2 with and without seeding using the Seed Mix. Large thin plates for peak 1 were observed in the refinement screen with MMS (0.1 *M* sodium acetate pH 4.5, 26% PEG 3350, 1 *M* LiCl) and these diffracted weakly (Fig. 4*a*). The refinement screen with peak 2 gave crystals from 0.1 *M* sodium acetate pH 4.5, 2.54 *M* ammonium sulfate and 5% PEG 400. The space group was *C*2, with large unit-cell parameters (a = 363, b = 132, c = 154 Å), a high solvent content (85%) and very anisotropic diffraction (∼10 Å and 4.5 Å).

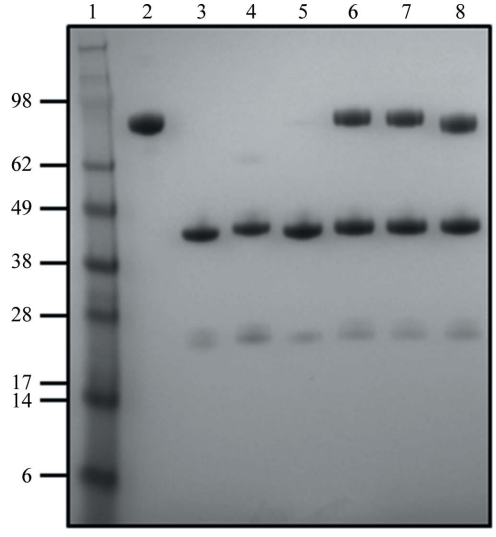

Figure 3
SDS–PAGE gel of TLR3 and complexes. Lane 1, molecular-weight marker (kDa); lane 2, TLR3 ECD; lane 3, Fab1068; lane 4, Fab12; lane 5, Fab15; lane 6, TLR3+3Fab peak 1; lane 7, TLR3+3Fab peak 2; lane 8, deglycosylated TLR3+3Fab.

In order to further improve crystal quality, an additive screen was performed using the most promising conditions from the refinement screen. This was carried out for peak 1 and peak 2 with Hampton Additive Screen combined with seeding using the Seed Mix and with 0.1 *M* sodium acetate pH 4.5, PEG 3350, 1 *M* LiCl and 0.1 *M* sodium acetate pH 4.5, 2.8 *M* ammonium sulfate as reservoir solutions. After additive screening there was no improvement in diffraction quality for peak 2 under ammonium sulfate or PEG 3350 conditions. After about one month, peak 1 gave a crystal in 0.1 *M* sodium acetate pH 4.5, 28% PEG 3350, 1 *M* LiCl and 20 m*M* Gly-Gly-Gly (GGG) (Fig. 4*b*). The crystal diffracted to 5.0 Å resolution and belonged to space group *C*2 with one molecule per asymmetric unit, 71% solvent content and smaller unit-cell parameters (a = 215, b = 142, c = 125 Å) than those of the peak 2 crystal (Fig. 4*c*). The structure of the quaternary complex was determined from the peak 1 crystal by molecular replacement using the published TLR3 structure (Bell *et al.*, 2005; Choe *et al.*, 2005) and structures of the Fabs (Luo *et al.*, 2010, manuscript in preparation).

4. Conclusions

We have shown that fine purification, microseed matrix screening and additive screening led to the successful crystallization of a complex of the TLR3 ECD with three different Fabs. Shallow-gradient anion-exchange purification with a strong anion-exchange resin (such as Mono Q) is capable of separating species with slight differences in charge arising from even single amino-acid changes, alterations in folding or post-translational modifications (Ahrer & Jungbauer, 2006; Chicz & Regnier, 1989; de la Calle Guntiñas *et al.*, 2004). The differently charged or folded species of the TLR3+3Fab complex were resolved into two peaks under these conditions. We were unable to identify molecular differences between peak 1 and peak 2 by mass spectrometry because the heavy glycosylation of the TLR3 molecule gives spectra that were difficult to interpret. Nonetheless, the peak 1 and peak 2 complexes were distinguishable in their crystallizability, yielding crystals under different conditions with different unit-cell parameters and solvent content. We have found the approach of ion exchange with a shallow gradient and low protein loading to be very successful in improving sample homogeneity, the number of hits and crystal quality for many different proteins and complexes.

Crystallization of the TLR3 quaternary complex was dependent on MMS. The role of seeds in promoting crystal growth was tested by performing control experiments with seeding stabilization solution only. Clear drops were observed when only seeding solution was added, whereas crystals grew when seeds were introduced into the crystallization mixture. This demonstrates that the microcrystalline seeds promote crystal formation for the TLR3+3Fab complex. Seeds that produced diffraction-quality crystals were a mixture of ammonium sulfate and sodium formate conditions that gave rise to crystals in PEG 3350 conditions. This supports the utility of MMS for producing diffraction-quality crystals (D'Arcy *et al.*, 2007; Ireton & Stoddard, 2004; Obmolova *et al.*, 2010).

Additives have been shown to promote productive crystal contacts or inhibit destructive contacts (Cudney *et al.*, 1994) by acting as electrostatic cross-linkers. Combining microseeding with additives is a strategy for a situation where seeds promote nucleation but diffraction quality or size is not sufficient (Bergfors, 2003; Walter *et al.*, 2008). In this study, the additive GGG improved diffraction to a point suitable for structure determination. In the absence of GGG crystals

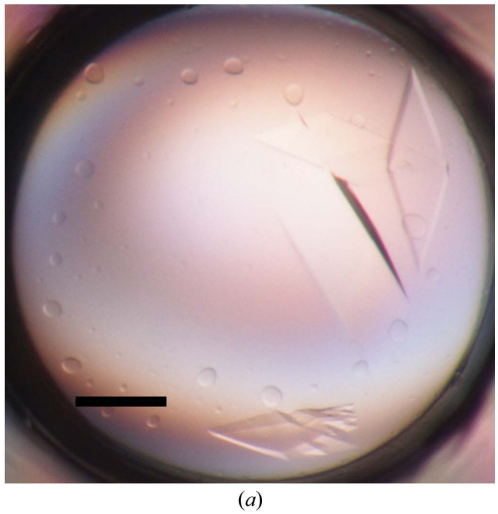

(*a*)

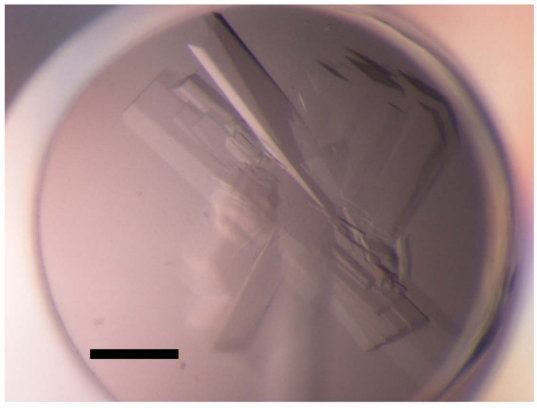

(*b*)

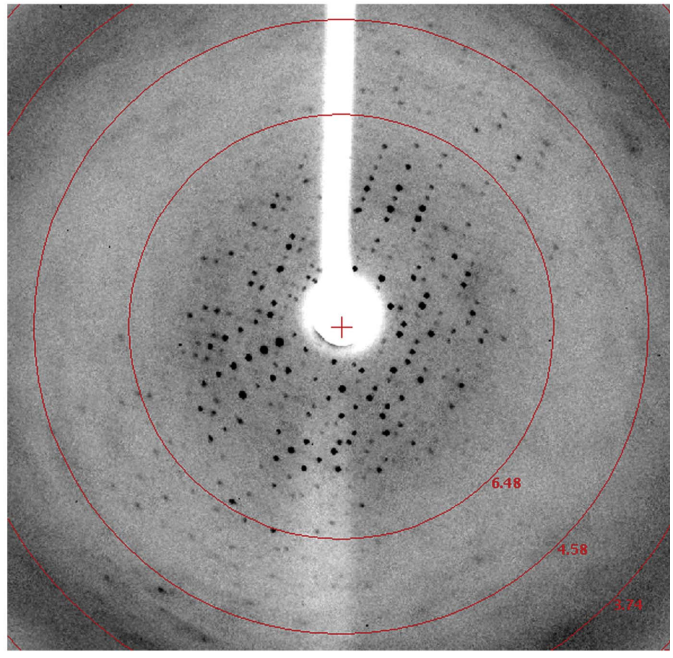

(*c*)

Figure 4
(*a*) Crystals of TLR3+3Fab peak 1 in 0.1 *M* sodium acetate pH 4.5, 26% PEG 3350, 1 *M* LiCl. (*b*) Crystals of TLR3+3Fab peak 1 in 0.1 *M* sodium acetate pH 4.5, 28% PEG 3350, 1 *M* LiCl and 30 m*M* Gly-Gly-Gly. Scale bars are 0.2 mm in length. (*c*) Diffraction image for the TLR3+3Fab peak 1 complex. Resolution rings are shown at 6.48, 4.58 and 3.74 Å.

derived from peak 1 in the same precipitant composition (0.1 *M* sodium acetate pH 4.5, PEG 3350, 1 *M* LiCl) diffracted to only ∼10 Å resolution. In the presence of GGG the resulting crystals diffracted to 5.0 Å resolution.

We did not obtain crystals of TLR3 alone or in complex with any of the antibodies under the conditions described for previous structures of TLR3 (Bell *et al.*, 2005; Botos *et al.*, 2009). The TLR3 used in this study was expressed in Sf9 cells, in contrast to the High Five cells used in the previous reports. It may be that a difference in the glycosylation pattern between the two insect strains accounts for the differential crystallizability observed. It is possible that the success with the TLR3+3Fab complex but not the complexes with one or two of the Fabs was because the three Fabs more efficiently masked regions of glycosylation that hindered crystal formation. Alternatively, it is possible that the complex with only one or two Fabs could not assemble in a geometry that facilitated three-dimensional crystal growth. Whatever the explanation, we attribute the success of the crystallization of the TLR3 complex to the use of multiple Fabs, which act as crystallization chaperones. Single (Hunte & Michel, 2002; Rasmussen *et al.*, 2007; Röthlisberger *et al.*, 2004; Zhou *et al.*, 2001) and two (Smith *et al.*, 2010) antibody Fab fragments have been used with some success as crystallization chaperones for difficult targets. Here, we extend the complexity to three noncompeting Fabs to obtain diffraction-quality crystals. Thus, the use of multiple Fabs as chaperones may prove to be valuable for crystallization of difficult targets such as membrane, multi-domain and heavily glycosylated proteins.

We thank Bethany Swencki-Underwood and other members of the Molecular Biology Group at Centocor for protein-production support, Suparna Paul and Bingyuan Wu for purification of Fabs, Steve Pomerantz for mass spectrometry and Lani San Mateo for project support.

References

Ahrer, K. & Jungbauer, A. (2006). *J. Chromatogr. B Analyt. Technol. Biomed. Life Sci.* **841**, 110–122.
Alexopoulou, L., Holt, A. C., Medzhitov, R. & Flavell, R. A. (2001). *Nature (London)*, **413**, 732–738.
Bell, J. K., Botos, I., Hall, P. R., Askins, J., Shiloach, J., Segal, D. M. & Davies, D. R. (2005). *Proc. Natl Acad. Sci. USA*, **102**, 10976–10980.
Benvenuti, M. & Mangani, S. (2007). *Nature Protoc.* **2**, 1633–1651.
Bergfors, T. (2003). *J. Struct. Biol.* **142**, 66–76.
Botos, I., Liu, L., Wang, Y., Segal, D. M. & Davies, D. R. (2009). *Biochim. Biophys. Acta*, **1789**, 667–674.
Calle Guntiñas, M. B. de la, Bordin, G. & Rodriguez, A. R. (2004). *Anal. Bioanal. Chem.* **378**, 383–387.
Chayen, N. E. & Saridakis, E. (2008). *Nature Methods*, **5**, 147–153.
Chicz, R. M. & Regnier, F. E. (1989). *Anal. Chem.* **61**, 2059–2066.
Choe, J., Kelker, M. S. & Wilson, I. A. (2005). *Science*, **309**, 581–585.
Cudney, R., Patel, S., Weisgraber, K., Newhouse, Y. & McPherson, A. (1994). *Acta Cryst.* D**50**, 414–423.
D'Arcy, A., Villard, F. & Marsh, M. (2007). *Acta Cryst.* D**63**, 550–554.
Duffy, K. E., Lamb, R. J., San Mateo, L. R., Jordan, J. L., Canziani, G., Brigham-Burke, M., Korteweg, J., Cunningham, M., Beck, H. S., Carton, J., Giles-Komar, J., Duchala, C., Sarisky, R. T. & Mbow, M. L. (2007). *Cell. Immunol.* **248**, 103–114.
Hunte, C. & Michel, H. (2002). *Curr. Opin. Struct. Biol.* **12**, 503–508.
Ireton, G. C. & Stoddard, B. L. (2004). *Acta Cryst.* D**60**, 601–605.
Koide, S. (2009). *Curr. Opin. Struct. Biol.* **19**, 449–457.
Kovari, L. C., Momany, C. & Rossmann, M. G. (1995). *Structure*, **3**, 1291–1293.
Luo, J., Obmolova, G., Huang, A., Strake, B., Teplyakov, A., Malia, T., Muzammil, S., Zhao, Y., Gilliland, G. L. & Feng, Y. (2010). *J. Mol. Biol.* **402**, 708–719.
McPherson, A. (2004). *Methods*, **34**, 254–265.
Obmolova, G., Malia, T. J., Teplyakov, A., Sweet, R. & Gilliland, G. L. (2010). *Acta Cryst.* D**66**, 927–933.
Pflugrath, J. W. (1999). *Acta Cryst.* D**55**, 1718–1725.
Rasmussen, S. G., Choi, H. J., Rosenbaum, D. M., Kobilka, T. S., Thian, F. S., Edwards, P. C., Burghammer, M., Ratnala, V. R., Sanishvili, R., Fischetti, R. F., Schertler, G. F., Weis, W. I. & Kobilka, B. K. (2007). *Nature (London)*, **450**, 383–387.
Röthlisberger, D., Pos, K. M. & Plückthun, A. (2004). *FEBS Lett.* **564**, 340–348.
Smith, B. J., Huang, K., Kong, G., Chan, S. J., Nakagawa, S., Menting, J. G., Hu, S.-Q., Whittaker, J., Steiner, D. F., Katsoyannis, P. G., Ward, C. W., Weiss, M. A. & Lawrence, M. C. (2010). *Proc. Natl Acad. Sci. USA*, **107**, 6771–6776.
Walter, T. S., Mancini, E. J., Kadlec, J., Graham, S. C., Assenberg, R., Ren, J., Sainsbury, S., Owens, R. J., Stuart, D. I., Grimes, J. M. & Harlos, K. (2008). *Acta Cryst.* F**64**, 14–18.
Zhao, Y., Gutshall, L., Jiang, H., Baker, A., Beil, E., Obmolova, G., Carton, J., Taudte, S. & Amegadzie, B. (2009). *Protein Expr. Purif.* **67**, 182–189.
Zhou, Y., Morais-Cabral, J. H., Kaufman, A. & MacKinnon, R. (2001). *Nature (London)*, **414**, 43–48.